Feasibility of direct utilization of biomass gasification product gas fuels in tubular solid oxide fuel cells for on-site electricity generation

Kongfa Chen,[a,b] Lan Zhang,[c] Na Ai,[a] Shu Zhang,[a] Yao Song,[a] Yuncai Song,[a] Qun Yi,[a]

Chun-Zhu Li,[a] and San Ping Jiang *,[a,b]

[a] Fuels and Energy Technology Institute, Curtin University, Perth, WA 6102, Australia

[b] Department of Chemical Engineering, Curtin University, Perth, WA 6102, Australia

[c] Energy Research Institute, Nanyang Technological University, Singapore 637553, Singapore

*Corresponding author: Phone: +61 8 9266 9804; Fax: +61 8 9266 1133; E-mail: s.jiang@curtin.edu.au (SP Jiang)

ABSTRACT: Biomass is one of the most abundant and cheap renewable energy sources and gasification product gases from the pyrolysis process of biomass such as mallee wood and wheat straw contain typically 20-27% H_2 and small amount of CO and CH_4 (8-13%). Here, preliminary results on the performance of Ni/Y_2O_3-ZrO_2 cermet anode-supported tubular solid oxide fuel cells (SOFCs) for the electricity generation from gasification product gases are presented. Two product gases derived from mallee wood and wheat straw are used as the fuels. The tubular SOFCs deliver a maximum power density over 576 mW cm^{-2} at 800°C, close to the power density based on the equivalent amount of pure H_2 or CH_4 fuel. The power density is affected by the flow rate of product gas, but there are no significant differences of power output among the product gas sources used. However, the cell performance decreases gradually and the degradation in the electricity generation performance of the tubular SOFC is most likely due to the presence of impurities such as sulphur and chlorine-containing compounds in the biomass feedstock. The results demonstrate the feasibility of the

gasification product gases fueled SOFCs for the on-site electricity generation and the deterioration effect of impurities could be mitigated by cleaning the product gases or by developing the contaminant tolerant electrodes.

Keywords: Tubular solid oxide fuel cells; gasification product gas; biogas; wheat straw; mallee woods; electricity generation.

1. INTRODUCTION

Biomass is one of the cheapest and abundant renewable energy sources. Compared to the traditional technologies based on the direct combustion of solid fuels, gasification-based power generation technologies can offer much higher efficiencies and lower emission of air pollutants (NO_x, SO_x, etc). The advantages of gasification are particularly profound for the utilisation of biomass, because biomass has a much higher gasification reactivity than coal and petroleum coke. Biomass gasification product gases are a complex mixture including hydrogen, methane, carbon monoxide, carbon dioxide, nitrogen and traces of impurities such as hydrogen sulphide, chlorine, ammonia and volatile organic compunds.[1-3] The composition of biogas is dependent on the type of biomass and production processes.[4] With small scale biomass gasifiers, fuel cells are the device of choice to generate electricity using the gasification product gas fuel due to the high efficiency and modularity of fuel cells. Among different types of fuel cells, solid oxide fuel cell (SOFC) is particularly suitable because of its flexibility to accept mixed fuel gases in addition to hydrogen, and is considered to be the most efficient and less polluting power generating technology. As an all-solid device, SOFC converts electrochemically the chemical energy of fuels such as H_2, CO and CH_4 directly to electricity without combustion.

There have been investigations on the direct utilization of gasification product gas or biogas fuel in SOFCs. Staniforth and Ormerod studied the effect of methane ratio in simulated biogas

CH_4-CO_2 mixture on the performance of tubular SOFC, and found that SOFC can be running on a remarkably low concentration of methane, on which the conventional heat engine cannot work.[5] Xie *et al.* evaluated the Ni–SDC anode-supported cell running on simulated N_2-H_2-CH_4-CO-CO_2 biogas at 600°C, and observed that the cell performance decreased rapidly within 20 min due to carbon deposition on the anode, whereas the cell stability was enhanced by alloying Ni with Cu.[6] The impurities in biogas such as H_2S in bio-waste derived gas have a profound effect on the anode activity and performance stability.[7-11] Shiratori *et al.* reported that the addition of 1 ppm H_2S to simulated CH_4-CO_2 biogas mixture caused a ~9% drop of cell voltage and a ~40% decrease in reaction rate of internal dry reforming reaction in the first 2 h of test at 1000 °C.[12] On the other hand, the sulphur poisoning effect can be minimized by desulphurization of the biogas[11, 13] or by tailoring the materials or composition of anodes.[9, 14, 15] In contrast to the dramatic performance degradation in the presence of H_2S, SOFCs are tolerant toward the presence of ammonia in the biogas which can be decomposed to nitrogen and water after the electrochemical reaction.[16]

However, there is a lack of information on performance of SOFCs on real biogas derived from the gasification of biomass as majority of the literatures are based on the simulated biogas compositions. Herein, we present our preliminary results on SOFC running on real biogases prepared from mallee wood and wheat straw by gasification. The results indicate the feasibility of direct utilization of the gasification product gases as the fuel of SOFCs for the on-site electricity generation.

2. EXPERIMENTAL SECTION

A laboratory-scale pilot gasification plant (H1.50 m × Φ0.44 m)[1, 17] was used for producing biogases in this study. The biomass samples were 0-6 mm with ~5% moisture. The details of the internal structure of mallee wood and wheat straw were given in reference 1.

Briefly, Australian mallee wood or wheat straw was continuously fed into the reactor and the average gasification temperature used in this study was ~880 ^{o}C. The gas products of the biomass were reformed by passing through a catalytic reactor embedded on the top part of the gasification plant. The char catalysts (4-6 mm) used in the catalytic reactor were separately prepared by pyrolysis of mallee chips at ~780 ^{o}C in the plant prior to the gasification experiments. The gasification products after going through the catalytic reactor were further cleaned by a series of bubblers (impingers) with chloroform and methanol (chloroform:methanol=4:1 in vol.). The bubblers were cooled in a dry ice bath (-78 ^{o}C). The gas coming out of the bubblers was then collected into gas bags and ready for use. The gas composition was in the range of 20-27% H_2, 5-8% CO, 3-5% CH_4, 8-10% CO_2 and 50-64% N_2. As-prepared biogases from mallee wood and wheat straw before being reformed by the char catalyst were denoted as B1 and B2, respectively, and as A1 and A2 after being reformed by the char catalyst. Table 1 lists the compositions of product gases in this study. The sulphur and chlorine-contained compounds were not analysed in this study. Nevertheless, when collecting the product gas, the strong sulfur was smelled, indicating the existence of sulfur in the gasification product gases.

NiO-yttria stabilized zirconia (YSZ) anode-supported YSZ film tubular SOFCs were fabricated by slip casting and dip coating methods. The weight ratio of NiO to YSZ powder was 65:35. Cathode layer consisting of a $La_{0.80}Sr_{0.20}MnO_3$-YSZ (LSM-YSZ with weight ratio of 1:1) composite cathode and a LSM current collection layer were applied to the sintered tube by dip coating and painting, followed by sintering at 1000°C for 2 h. The fabrication details were given in a previous report.[18] The cell areas were 3.0 to 3.7 cm^2. Ag ink (DAD-87, Shanghai Research Institute of Synthetic Resin) was painted on both the anode and cathode as current collector. The tubular cell was sealed to an alumina tube via a ceramic sealant (Ceramabond 552, Aermco Products Inc.). Hydrogen, methane or biogases were

passed through a water bubbler at room temperature and water content in wet fuels was ~3%. The fuel flow rate was varied from 25 to 100 ml min^{-1}. NiO of the anode was reduced to Ni metal in situ under fuel reducing conditions before the tests at 800 ^{o}C, forming Ni-YSZ cermets. The cathode was exposed directly to ambient air.

The cell performance was measured at 800°C using a Gamry Reference 3000 Potentiostat. The electrochemical impedance spectroscopy of the cell was measured at open circuit in the frequency range of 0.1 Hz to 100 kHz with a signal amplitude of 10 mV. Cell microstructure was examined by scanning electron microscopy (SEM, Zeiss Neon 40EsB) equipped with X-ray energy dispersion spectroscopy (EDS). Figure 1 shows the cell arrangement and tubular cell used in this study.

3. RESULTS AND DISCUSSION

3.1. Cell structure. Figure 2 shows the SEM micrographs of a typical tubular cell structure. The cell consists of 5 layers including a 0.8 mm Ni-YSZ porous anode support with a coarse structure, a 13 µm-thick anode functional layer (AFL) with a fine microstructure, a 16 µm-thick dense YSZ electrolyte film, a 14 µm-thick porous LSM-YSZ composite cathode functional layer (CFL) and a 8 µm-thick porous LSM outer cathodic current collection layer (CCCL). The functional layer of an electrode is where the electrochemical reaction occurs and the fine and uniform microstructure maximizes the active sites at the electrode/electrolyte interface region and facilitates the electrochemical reaction, while the coarse and porous outer layer benefits the fast gas diffusion of the reactants and products of the fuel cell reaction to and from the reaction sites primarily located within the inner functional layers.

3.2. Cell performance in wet H_2 and wet CH_4. The polarization performance of the anode-supported tubular cells was first investigated in pure wet hydrogen and methane. Hydrogen and methane are the main components of the biogases, as shown in Table 1. Figure

3 shows the performance curves of a tubular cell running on pure wet hydrogen and wet methane at 800°C. The open circuit voltage of the cell in wet H$_2$ is ~1.1 V (Fig. 3a), close to the theoretical value, indicating that the electrolyte film is fully dense and gas impermeable. The power density at a cell voltage of 0.7 V was 523 mW cm^{-2} at a hydrogen flow rate of 50 ml min^{-1}, and increased to 598 and 630 mW cm^{-2} when the fuel flow rate was increased to 100 and 200 ml min^{-1}, respectively. The impedance responses of the cell were characterized by two discernible arcs at high (> 10 Hz) and low (< 10 Hz) frequencies (Fig. 3b), indicating that the cell reaction can be separated by at least two dominant electrode processes. The low frequency arc depends strongly on the flow rate of fuel and is reduced by increasing the hydrogen flow rate, while the high frequency arc remains more or less the same with the fuel flow rate. This indicates that the low frequency arc is most likely associated with the electrochemical oxidation reaction of the hydrogen at the Ni-YSZ anode and the high frequency arc is associated with the oxygen reduction reaction at the LSM-YSZ cathode. This is consistent with the observation of the characteristic cathodic impedance at a high frequency of 2 kHz for a LSM-YSZ cathode and the characteristic anodic impedance at a low frequency of 4 Hz for a Cu-ceria-YSZ anode.[19] During the hydrogen oxidation reaction, hydrogen is consumed at the reactive sites primarily within the Ni-YSZ function layer with the concomitant production of water. Thus, a higher fuel flow rate facilitates the rapid transport of fuel and removal of the reaction product to and from the function layer at the electrode/electrolyte interface region.

In the case of wet CH$_4$, the open circuit voltage of the cell is similar to that measured in wet H$_2$. The power density measured at 0.7 V is 583 mW cm^{-2} in CH$_4$, higher than 523 mW cm^{-2} measured in wet H$_2$ under the same flow rate (Fig. 3c). This indicates the high electrocatalytic activity of the Ni-YSZ anode for the oxidation reaction of methane.[20, 21] Compared to the case of running on wet hydrogen, the low frequency impedance responses

6

associated with the methane oxidation reaction at the anode are very different. The low frequency impedances are characterized by more than one arc and also are significantly smaller than that observed for the hydrogen oxidation reaction (Fig. 3d). This shows that methane oxidation reaction is a complicated and multiple step reaction and may consist of methane internal reforming, carbon deposition and oxidation under fuel cell operation conditions.[21-23] The thick anode layer (~0.8 mm) can retain the steam produced within the structure, which in turn could significantly enhance the internal reforming of methane, producing *in situ* H_2 and CO fuels for the fuel cell reaction. This appears to be confirmed by the high power output of the cells at high polarization currents. The steam produced within the electrode layer in turn suppresses the catalytic cracking of methane and carbon deposition. Nevertheless, the performance and stability of Ni-YSZ based cermet anodes is critically dependent on the composition and microstructure of anode, supply of oxygen ions by applying current, ratio of methane to steam, etc.[24]

Stability of the tubular SOFCs in wet H_2 and wet CH_4 was tested under a constant current of 500 mA cm^{-2} at 800 °C. In the case of running on hydrogen, the cell is more or less stable. The initial voltage was 0.81 V and was stabilized at 0.80 V after polarization at 800°C for 25 h (Fig. 4a). After switching to wet CH_4, the voltage increased abruptly and was 0.85 V after polarization for 2 h. After interruption of the current passage for the polarization and impedance measurements for ~5 min, the cell voltage started at ~0.90 V when the current was applied. However, the cell voltage was rapidly declined in the first 10 min, followed by a rather gradual decrease. Such rapid change of the cell voltage as a function of the interruption and application of polarization current is reproducible, but the general trend in the cell stability is not affected. After running on wet methane for 24 h, the voltage decreased slowly to 0.83 V, slightly lower than the initial cell voltage of 0.85 V. The cell voltage after switching to hydrogen is 0.77 V, lower than 0.80 V before the test in wet methane. This

indicates that the degradation in the cell performance in wet methane cannot be completely recovered. This is also indicated by the slightly reduced power output of the tubular cells after running on methane fuel (Fig. 4b and c). The results indicate that the tubular cells have an acceptable operating stability in wet hydrogen and methane.

3.3. Cell performance, fuel efficiency and stability in biogases. Figure 5 shows the polarization and power output curves of the tubular cells running on biogases at 800°C. The polarization performance of the tubular cells is largely dependent on the flow rate of biogases, similar to that on wet hydrogen. For example, the peak power density running on gasification product gas from wheat straw after the catalytic reforming, A2 biogas, is 265, 422 and 576 mW cm^{-2} at a flow rate of 25, 50 and 100 ml min^{-1}, respectively. An increase in the flow rate of the biogas increases the power output of the cell. The peak power density in the A1 and A2 biogases at a flow rate of 50 ml min^{-1} is 449 and 422 mW cm^{-2}, respectively, higher than 390 and 385 mW cm^{-2} in the B1 and B2 biogases. The increase of power output in the A1 and A2 biogases is most likely due to the small increase in the hydrogen and carbon monoxide contents of the reformates of the product gases B1 and B2 after the reforming treatment by the char catalysts (see Table 1). The power output of the tubular cells running on different fuels is summarized in Table 2.

The power density of tubular cells based on biogases is quite reasonable and also comparable to that measured in pure hydrogen and methane. For example, the cells running on biogases (H$_2$+CO+CH$_4$ <50%) at a flow rate of 100 ml min^{-1} deliver power densities of 435-459 mW cm^{-2} at a cell voltage of 0.7 V, slightly lower than 523 and 583 mW cm^{-2} on hydrogen and methane at a flow rate of 50 ml min^{-1}, respectively. The power output of the cells could be further increased by the increase in the fuel flow rate and by the optimization of the cell and electrode structures. The good power performance of the tubular SOFCs as

shown in the present study demonstrates that the biomass gasification product gases can be an effective fuel to replace pure hydrogen and methane for the electricity generation.

The fuel efficiency of tubular cells was also calculated at a cell voltage of 0.7 V and the results are given in Table 3. Fuel flow rate has a significant effect on the fuel efficiency. For example, the fuel efficiency is 38.8% at a fuel flow rate of 50 mL min^{-1} and decreases to 22.1% when the flow rate increases to 100 mL min^{-1}, though the power density increases at a higher flow rate for the hydrogen fuel (see Table 2). In the case of biogas A2 at a flow rate of 100 ml min^{-1} the fuel efficiency is 26.6% and 36.7% based on a N_2 content of 50% and 64%, respectively, lower than 38.9% in hydrogen but higher than 10.7% in methane at a flow rate of 50 ml min^{-1}. The presence of a high amount of non-flammable gases, i.e. N_2 and CO_2 dramatically dilutes the concentration of fuels, and therefore the cell output performance in biogases is slightly lower than that in pure hydrogen and methane. However, the efficiency calculated on small tubular cells is generally on the low side due to the much smaller reaction area as compared to the practical tubular and planar cells. The data as listed in Table 3 can only be used for the comparison purpose.

Figure 6 shows the short-term stability tests of tubular cells under a constant current of 200 mA cm^{-2} at 800°C. Prior to the test on wet biogases, the cell voltage was stabilized on wet H_2 at 0.96 V (Fig. 6a). The introduction of the reformate of gasification product gas from mallee wood, A1 biogas, leads to a rapid and continuous decrease of the cell voltage. The initial cell voltage was 0.91 V and declined to 0.85 V after polarization in A1 biogas for 150 min. On the other hand, the cell voltage can be fully recovered by switching back to H_2. In the case of running on the reformate of gasification product gas from wheat straw, A2 biogas, the cell voltage increased quickly from 0.79 V to 0.89 V after polarization for 50 min. The cell performance is rather stable and the cell voltage decreased slightly to 0.85 V after operation for 150 min (Fig. 6b). The cell performance measured in the gasification product

gas from wheat straw before the catalytic treatment, B2 biogas, shows a similar trend to A2, though the decay of voltage in B2 is more pronounced. Nevertheless, the degradation of tubular cells is much more significant as compared to that running on pure hydrogen and methane. However, similar to the case of A1 biogas, the cell performance losses after running on A2 and B2 were completely recovered after returning to H_2 fuel.

The impedance responses before and after the short-term stability tests on the biogases are shown in Fig. 7. After the stability tests in various biogases, there is little change in the high frequency arc, while the low frequency arc increases in size. As discussed above (Fig. 3), the low frequency impedance is associated with the electrochemical oxidation reaction of fuels at the anode. Thus, the increase in the low frequency arc of the tubular cells after polarization in the biogases is most likely due to the performance decay of the Ni-YSZ anode during the test in biogases.

3.4. Microstructure after stability tests in biogases. Figure 8 shows the SEM micrographs of cross section and surface of Ni-YSZ cermet anode electrodes after the stability tests in biogases at 800 ^{o}C. In the regions close to the Ni-YSZ electrode and YSZ electrolyte interface region, i.e., the anode function layer, the surface of both Ni and YSZ particles is clean after testing in various biogases (Fig. 8a and c). In contrast to the clean Ni grain surface in the bulk of the electrode, there are nanoparticles formed on the surface of Ni grains close to the outmost surface of the electrodes (Fig. 8b). Similar deposition and formation of nanoparticles were also observed on the surface of Ni particles after test in gasification product gases derived from mallee wood and wheat straw before the catalytic reforming treatment, B1 and B2 biogases. EDS was conducted on the Ni particles but cannot detect any other peaks except Ni probably due to the very low concentration of nanoparticles formed on the surface.

3.5. Feasibility of direct utilization of biogas fuel in tubular SOFC. Among the agricultural biomasses (wheat straw, triticale, fescue miscanthus and switchgrass), wheat straw has highest sulphur content of 1.6% and the chlorine content is also high, ~0.27%.[25] The sulphur and chlorine contents of mallee wood are lower, 0.01 and 0.04 wt%, respectively.[26] It has been reported that trace of H_2S even in the ppm level can poison the Ni anode by initial adsorption of sulphur onto Ni grain surface, followed by the formation of nickel sulphide (Ni_2S_3), which can significantly reduce the reaction site as well as the electrocatalytic activity for the oxidation reaction on the anode.[27] The sulphur poison of the electrocatalytic activity of Ni-YSZ cermet anodes has been reported to have an initial rapid cell voltage drop, followed by a slow but continuous drop in cell voltage. The initial sharp degradation is recoverable on removal of H_2S as a result of rapid desorption of sulphur on the Ni surface;[28, 29] while the second stage of poisoning due to the formation of nickel sulphide at the anode/electrolyte interface cannot be completely recovered.[30] Our previous study on sulphur deposition and poisoning of Ni-YSZ and Ni-GDC anodes reveals the significant modification and roughening of Ni particle surface after exposure to a H_2S concentration in a range of 5-700 ppm, though there is a lack of distinct sulphur peak in the EDS spectra.[8] The formation of nickel sulphide and its decomposition on pure hydrogen could be responsible for the modification and roughening of the Ni surface.[8] The presence of H_2S can be highly detrimental to the electrocatalytic activity of Ni catalysts.[7, 9, 10, 31] Staniforth and Kendall observed the rapid power output loss within 100 min when running the cells in raw landfill biogas which contains less than 1% H_2S, and they found that the desulphurisation significantly enhanced the cell longevity.[13] Chlorine compounds such as Cl_2 and HCl are also known to poison and degrade the activity of Ni-YSZ cermet anode.[32, 33] For example, Haga *et al*. found that the chlorine degradation rate increased with increasing Cl_2 concentration and observed the formation of Ni nanoparticles on zirconia grains.[32] The presence of H_2S in the

gasification product gases derived from mallee wood and wheat straw is the most likely reason for the degradation and loss of the activity and performance of the tubular cells. The presence of sulphur was also indicated by the strong smell of H_2S during the product gas collection in this study.

However, the near complete performance recoverability of the tubular cells after returning to hydrogen (Fig. 6) and negligible microstructure modification and roughening of the Ni phase of the Ni-YSZ cermet anodes after test in biogases (Fig. 8) indicate that poisoning of impurities in the biogases on the electrocatalytic activity can be recovered and damage to the microstructure of the Ni-YSZ cermet anodes is relatively minor, though the nature and content of the impurities in the biogases are not clear at this stage. As shown in the literature, the deterioration effect of H_2S can be mitigated by cleaning the product gases[11] or by developing sulphur tolerant anodes such as ceria nanoparticles infiltrated Ni-YSZ[8, 34, 35] and Cu-Co-ceria.[36] On the other hand, the poisoning effect of chlorine compounds is largely reversible.[32] Early studies also show that ceria and Pd infiltration can also significantly enhance the tolerance and resistance of the Ni-YSZ cermet anodes towards carbon cracking and deposition.[18, 20, 37] In addition, after the performance and performance stability test in gasification product gases, no carbon particles or layer was observed on the fuel entry section of the alumina tubes or on the surface of the anode side of the cell. This indicates that the carbon cracking or deposition of the gasification product gases under the present conditions is very low or negligible. Thus, with further microstructure modification and optimization, Ni-YSZ based tubular cells can be operated directly in gasification product gases with high power output and operating stability.

4. CONCLUSIONS

Mallee wood and wheat straw derived gasification product gases were investigated as the potential fuels for tubular SOFCs. The preliminary results have demonstrated that the SOFC running on the biogases can reach a peak power density of 576 mW cm^{-2} at 800°C, comparable to that running on equivalent amount of pure hydrogen or methane. The presence of impurities such as H_2S and Cl-containing compounds in the biogases deteriorates the microstructure and electrocatalytic activity of Ni-YSZ anode, but the performance can be recovered after returning to pure hydrogen. The results indicate that by removing the impurities in particular sulphur via desulphurisation and/or by developing sulphur-tolerant anodes, it is feasible to directly utilize biomass gasification product gases as effective fuels in SOFCs for the on-site electricity generation.

ACKNOWLEDGEMENTS

REFERENCES

1.   Dong, L.; Asadullah, M.; Zhang, S.; Wang, X. S.; Wu, H. W.; Li, C. Z., An advanced biomass gasification technology with integrated catalytic hot gas cleaning Part I. Technology and initial experimental results in a lab-scale facility. *Fuel* **2013,** 108, 409-416.
2.   Rasi, S.; Veijanen, A.; Rintala, J., Trace compounds of biogas from different biogas production plants. *Energy* **2007,** 32, (8), 1375-1380.
3.   Nielsen, H. B.; Angelidaki, I., Strategies for optimizing recovery of the biogas process following ammonia inhibition. *Bioresource Technology* **2008,** 99, (17), 7995-8001.
4.   Herout, M.; Malaťák, J.; Kučera, L.; Dlabaja, T., Biogas composition depending on the type of plant biomass used. *Research in Agricultural Engineering* **2011,** 57, (4), 137-143.

5.   Staniforth, J.; Ormerod, R. M., Implications for using biogas as a fuel source for solid oxide fuel cells: internal dry reforming in a small tubular solid oxide fuel cell. *Catal. Lett.* **2002,** 81, (1-2), 19-23.

6.   Xie, Z.; Xia, C. R.; Zhang, M. Y.; Zhu, W.; Wang, H. T., Ni1-xCux alloy-based anodes for low-temperature solid oxide fuel cells with biomass-produced gas as fuel. *J. Power Sources* **2006,** 161, (2), 1056-1061.

7.   Rasmussen, J. F. B.; Hagen, A., The effect of H2S on the performance of Ni–YSZ anodes in solid oxide fuel cells. *Journal of Power Sources* **2009,** 191, (2), 534-541.

8.   Zhang, L.; Jiang, S. P.; He, H. Q.; Chen, X. B.; Ma, J.; Song, X. C., A comparative study of H2S poisoning on electrode behavior of Ni/YSZ and Ni/GDC anodes of solid oxide fuel cells. *Int. J. Hydrog. Energy* **2010,** 35, (22), 12359-12368.

9.   Xu, C.; Zondlo, J. W.; Gong, M.; Elizalde-Blancas, F.; Liu, X.; Celik, I. B., Tolerance tests of H2S-laden biogas fuel on solid oxide fuel cells. *Journal of Power Sources* **2010,** 195, (15), 4583-4592.

10.   Laycock, C. J.; Staniforth, J. Z.; Ormerod, R. M., Biogas as a fuel for solid oxide fuel cells and synthesis gas production: effects of ceria-doping and hydrogen sulfide on the performance of nickel-based anode materials. *Dalton Transactions* **2011,** 40, (20), 5494-5504.

11.   Shiratori, Y.; Ijichi, T.; Oshima, T.; Sasaki, K., Internal reforming SOFC running on biogas. *Int. J. Hydrog. Energy* **2010,** 35, (15), 7905-7912.

12.   Shiratori, Y.; Oshima, T.; Sasaki, K., Feasibility of direct-biogas SOFC. *International Journal of Hydrogen Energy* **2008,** 33, (21), 6316-6321.

13.   Staniforth, J.; Kendall, K., Cannock landfill gas powering a small tubular solid oxide fuel cell — a case study. *Journal of Power Sources* **2000,** 86, (1–2), 401-403.

14.   Zheng, L. L.; Wang, X.; Zhang, L.; Wang, J.-Y.; Jiang, S. P., Effect of Pd-impregnation on performance, sulfur poisoning and tolerance of Ni/GDC anode of solid oxide fuel cells. *International Journal of Hydrogen Energy* **2012,** 37, (13), 10299-10310.

15.   Kurokawa, H.; Yang, L.; Jacobson, C. P.; De Jonghe, L. C.; Visco, S. J., Y-doped SrTiO3 based sulfur tolerant anode for solid oxide fuel cells. *Journal of Power Sources* **2007,** 164, (2), 510-518.

16.   Staniforth, J.; Ormerod, R. M., Running solid oxide fuel cells on biogas. *Ionics* **2003,** 9, (5-6), 336-341.

17.   Zhang, S.; Asadullah, M.; Dong, L.; Tay, H. L.; Li, C. Z., An advanced biomass gasification technology with integrated catalytic hot gas cleaning. Part II: Tar reforming using char as a catalyst or as a catalyst support. *Fuel* **2013,** 112, 646-653.

18.   Zhang, L.; He, H. Q.; Kwek, W. R.; Ma, J.; Tang, E. H.; Jiang, S. P., Fabrication and Characterization of Anode-Supported Tubular Solid-Oxide Fuel Cells by Slip Casting and Dip Coating Techniques. *J. Am. Ceram. Soc.* **2009,** 92, (2), 302-310.

19.   McIntosh, S.; Vohs, J. M.; Gorte, R. J., Impedance spectroscopy for the characterization of Cu-Ceria-YSZ anodes for SOFCs. *J. Electrochem. Soc.* **2003,** 150, (10), A1305-A1312.

20.   Wang, W.; Jiang, S. P.; Tok, A. I. Y.; Luo, L., GDC-impregnated Ni anodes for direct utilization of methane in solid oxide fuel cells. *J. Power Sources* **2006,** 159, (1), 68-72.

21.   Ahmed, K.; Foger, K., Kinetics of internal steam reforming of methane on Ni/YSZ-based anodes for solid oxide fuel cells. *Catal. Today* **2000,** 63, (2-4), 479-487.

22.   Eigenbrodt, B. C.; Pomfret, M. B.; Steinhurst, D. A.; Owrutsky, J. C.; Walker, R. A., Direct, In Situ Optical Studies of Ni-YSZ Anodes in Solid Oxide Fuel Cells Operating with Methanol and Methane. *Journal of Physical Chemistry C* **2011,** 115, (6), 2895-2903.

23.   Eguchi, K.; Kunisa, Y.; Kayano, M.; Sekizawa, K.; Yano, S.; Arai, H., Power generation characteristics of solid oxide fuel cell with internal steam reforming of methane. *Denki Kagaku* **1996,** 64, (6), 596-601.

24.   Chen, K.; Jiang, S. P., Degradation and Durability of Electrodes of Solid Oxide Fuel Cells. In *Materials for High-Temperature Fuel Cells*, Wiley-VCH Verlag GmbH & Co. KGaA: 2013; pp 245-307.

25.   Perez, D. D.; Dupont, C.; Guillemain, A.; Jacob, S.; Labalette, F.; Briand, S.; Marsac, S.; Guerrini, O.; Broust, F.; Commandre, J. M., Characterisation of the Most Representative Agricultural

and Forestry Biomasses in France for Gasification. *Waste and Biomass Valorization* **2015,** 6, (4), 515-526.

26.   Min, Z. H.; Yimsiri, P.; Asadullah, M.; Zhang, S.; Li, C. Z., Catalytic reforming of tar during gasification. Part II. Char as a catalyst or as a catalyst support for tar reforming. *Fuel* **2011,** 90, (7), 2545-2552.

27.   Gong, M. Y.; Liu, X. B.; Trembly, J.; Johnson, C., Sulfur-tolerant anode materials for solid oxide fuel cell application. *J. Power Sources* **2007,** 168, (2), 289-298.

28.   Zha, S. W.; Cheng, Z.; Liu, M. L., Sulfur poisoning and regeneration of Ni-based anodes in solid oxide fuel cells. *J. Electrochem. Soc.* **2007,** 154, (2), B201-B206.

29.   Brightman, E.; Ivey, D. G.; Brett, D. J. L.; Brandon, N. P., The effect of current density on H2S-poisoning of nickel-based solid oxide fuel cell anodes. *Journal of Power Sources* **2011,** 196, (17), 7182-7187.

30.   Ishikura, A.; Sakuno, S.; Komiyama, N.; Sasatsu, H.; Masuyama, N.; Itoh, H.; Yasumoto, K., Influence of H2S Poisoning on Anode Layer of SOFC. *Solid Oxide Fuel Cells 10 (Sofc-X), Pts 1 and 2* **2007,** 7, (1), 845-850.

31.   Cheng, Z.; Wang, J. H.; Choi, Y. M.; Yang, L.; Lin, M. C.; Liu, M. L., From Ni-YSZ to sulfur-tolerant anode materials for SOFCs: electrochemical behavior, in situ characterization, modeling, and future perspectives. *Energy & Environmental Science* **2011,** 4, (11), 4380-4409.

32.   Haga, K.; Shiratori, Y.; Ito, K.; Sasaki, K., Chlorine Poisoning of SOFC Ni-Cermet Anodes. *J. Electrochem. Soc.* **2008,** 155, (12), B1233-B1239.

33.   Li, T. S.; Xu, C.; Chen, T.; Miao, H.; Wang, W. G., Chlorine contaminants poisoning of solid oxide fuel cells. *J. Solid State Electrochem.* **2011,** 15, (6), 1077-1085.

34.   Trembly, J. P.; Marquez, A. I.; Ohrn, T. R.; Bayless, D. J., Effects of coal syngas and H2S on the performance of solid oxide fuel cells: Single-cell tests. *J. Power Sources* **2006,** 158, (1), 263-273.

35.   Kurokawa, H.; Sholklapper, T. Z.; Jacobson, C. P.; De Jonghe, L. C.; Visco, S. J., Ceria nanocoating for sulfur tolerant Ni-based anodes of solid oxide fuel cells. *Electrochem. Solid State Lett.* **2007,** 10, (9), B135-B138.

36.   Fuerte, A.; Valenzuela, R. X.; Escudero, M. J.; Daza, L., Study of a SOFC with a bimetallic Cu-Co-ceria anode directly fuelled with simulated biogas mixtures. *International Journal of Hydrogen Energy* **2014,** 39, (8), 4060-4066.

37.   Babaei, A.; Zhang, L.; Liu, E. J.; Jiang, S. P., Performance and carbon deposition over Pd nanoparticle catalyst promoted Ni/GDC anode of SOFCs in methane, methanol and ethanol fuels. *Int. J. Hydrog. Energy* **2012,** 37, (20), 15301-15310.
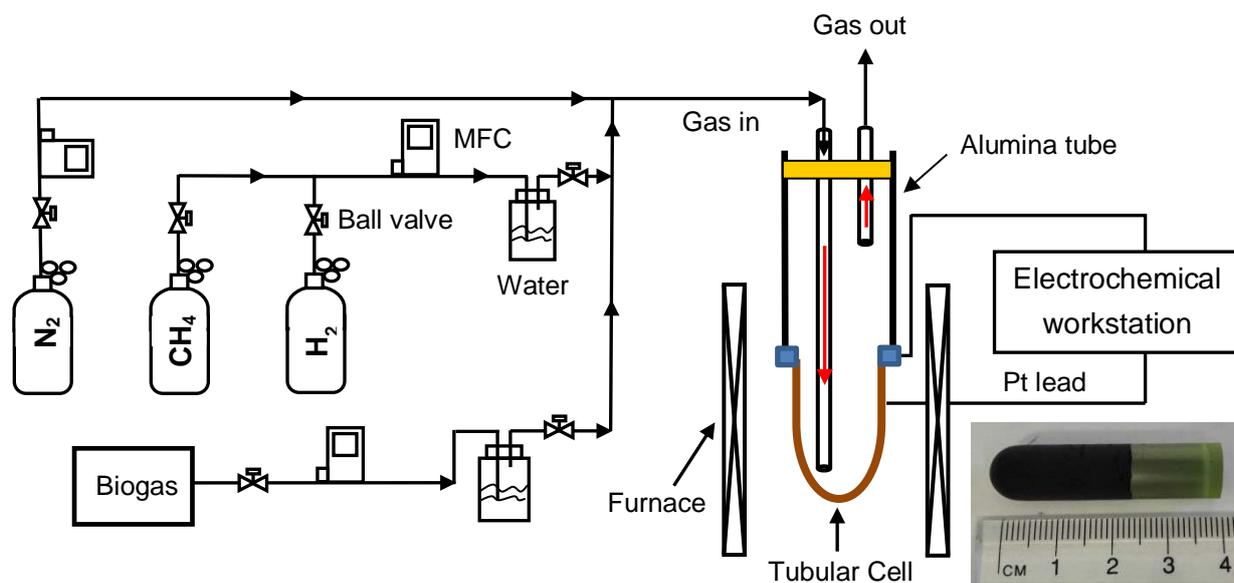
Figure 1. Schematic diagram of tubular cell arrangement for running on biogases. An optical

photo of a tubular cell is also included.
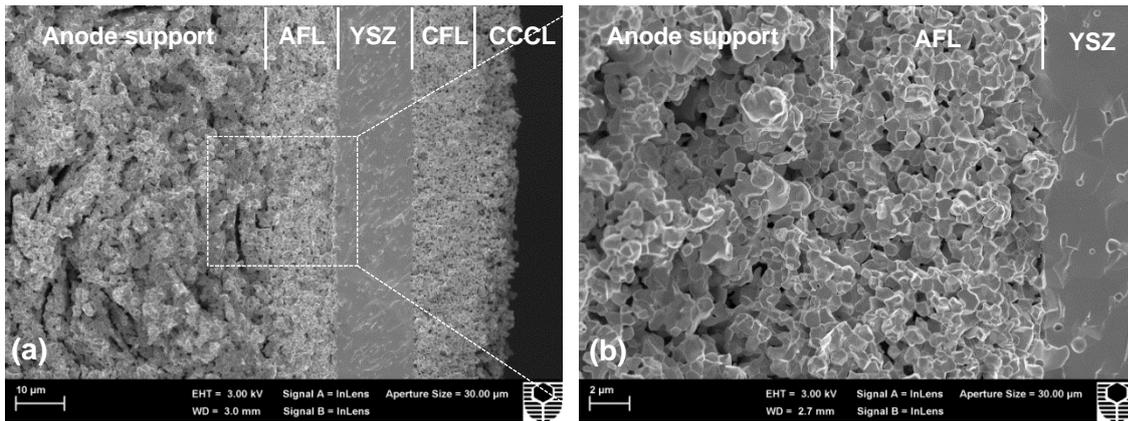
Figure 2. SEM micrographs of cross sections of a typical tubular cell: (a) Overview of 5 layered structure consisting of a 800 µm Ni-YSZ anode support, a 13 µm Ni-YSZ anode functional layer (AFL), a 16 µm YSZ electrolyte, a 14 µm LSM-YSZ cathode functional layer (CFL) and a 8 µm LSM cathode current collection layer (CCCL), and (b) magnified anode support/AFL/YSZ electrolyte triple layers.
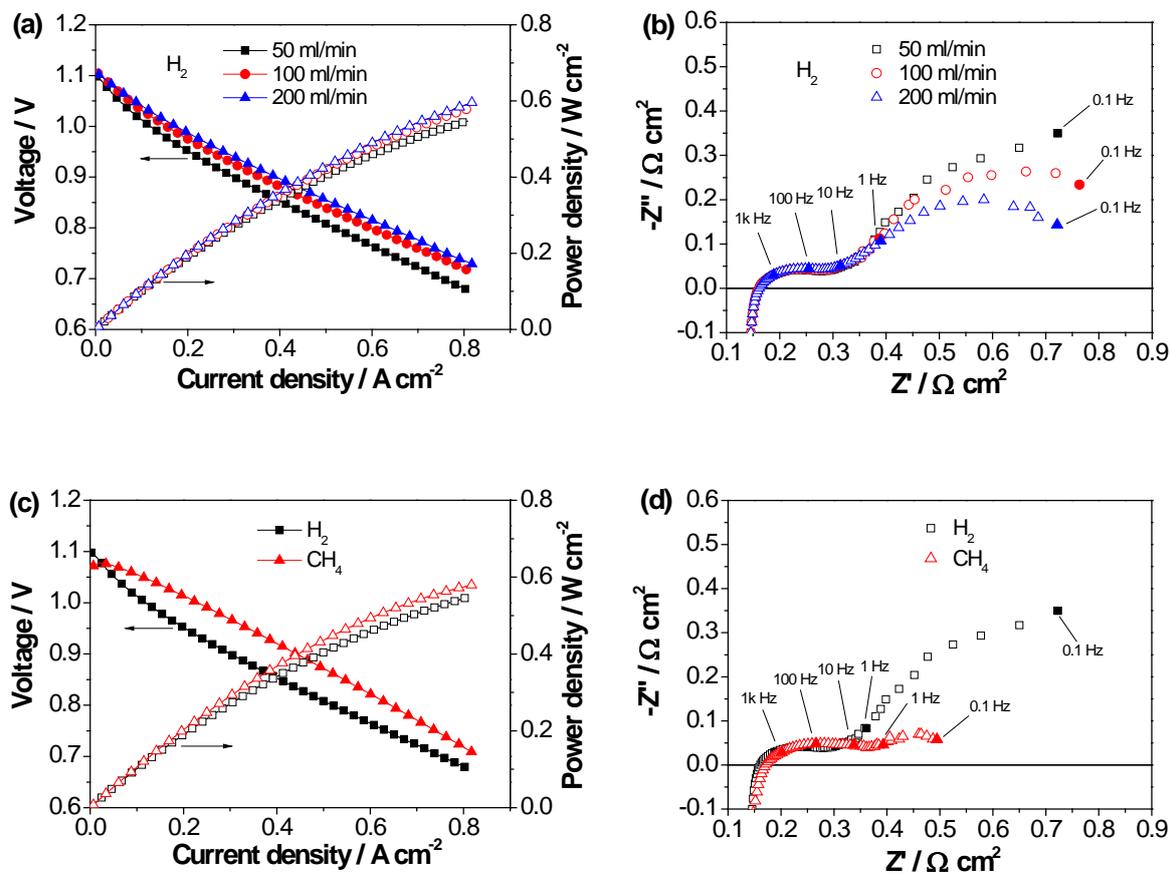
Figure 3. (a) Polarization performance curves and (b) impedance responses of a tubular cell running on wet H_2 at $800^{\circ}C$, measured at different flow rates, and comparisons of (c) polarization curves and (d) impedance responses of the cell running on wet H_2 and wet CH_4 at 50 ml min^{-1}.
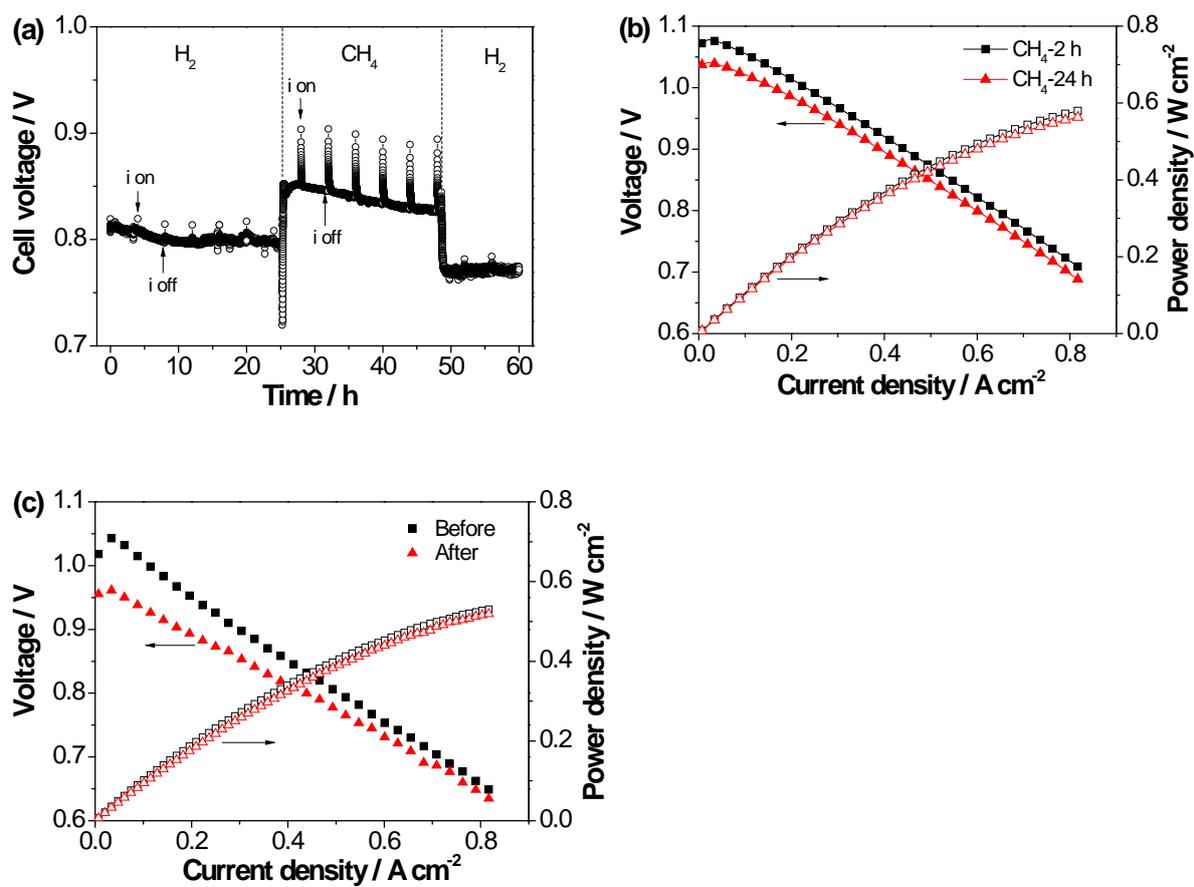
Figure 4. (a) Cell stability curve at a constant current of 500 mA cm^{-2} and 800°C in wet H$_2$ and wet CH$_4$ at a flow rate of 50 ml min^{-1}, and performance curves measured (b) in wet CH$_4$ and (c) in wet H$_2$ before and after running on CH$_4$.
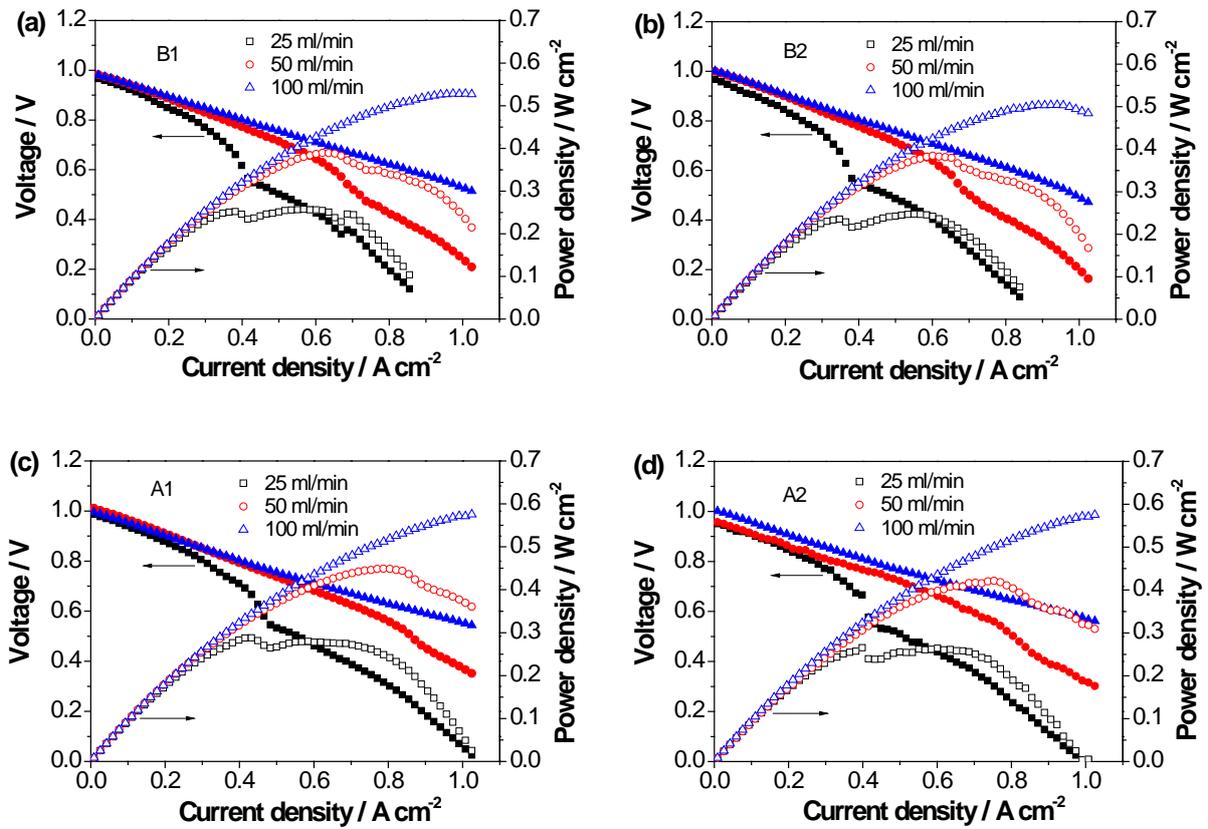
Figure 5. Polarization performance curves of a tubular cell in biogases: (a) B1, (b) B2, (c) A1 and (d) A2 at 800°C in the flow rate range of 25-100 ml min^{-1}.
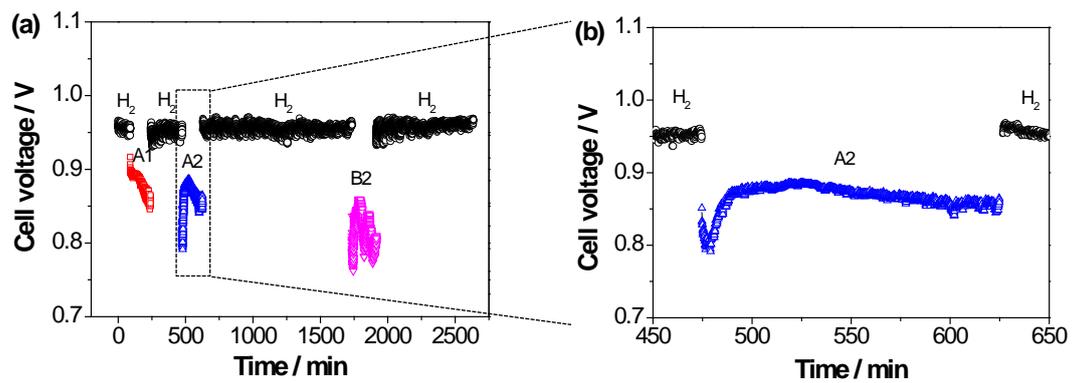
Figure 6. (a) Cell voltage as a function of current passage time at 200 mA cm^{-2} and 800°C in hydrogen and various biogases at a flow rate of 50 ml min^{-1} and (b) the enlarged stability curve in the cell in A2 biogas.
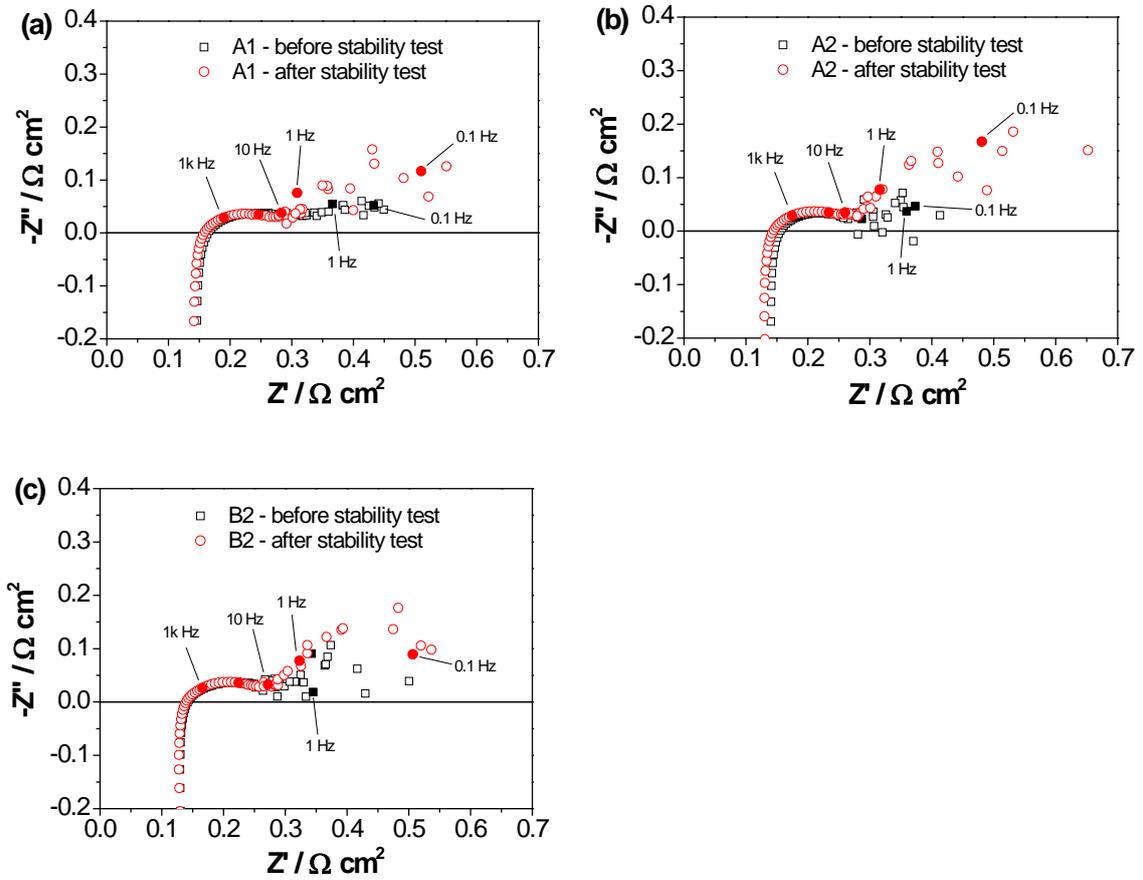
Figure 7. Impedance responses of a tubular cell before and after the stability tests in various biogases at a constant current of 200 mA cm^{-2}, 800°C for 150-180 min.

Near anode/electrolyte interface   Near outmost surface
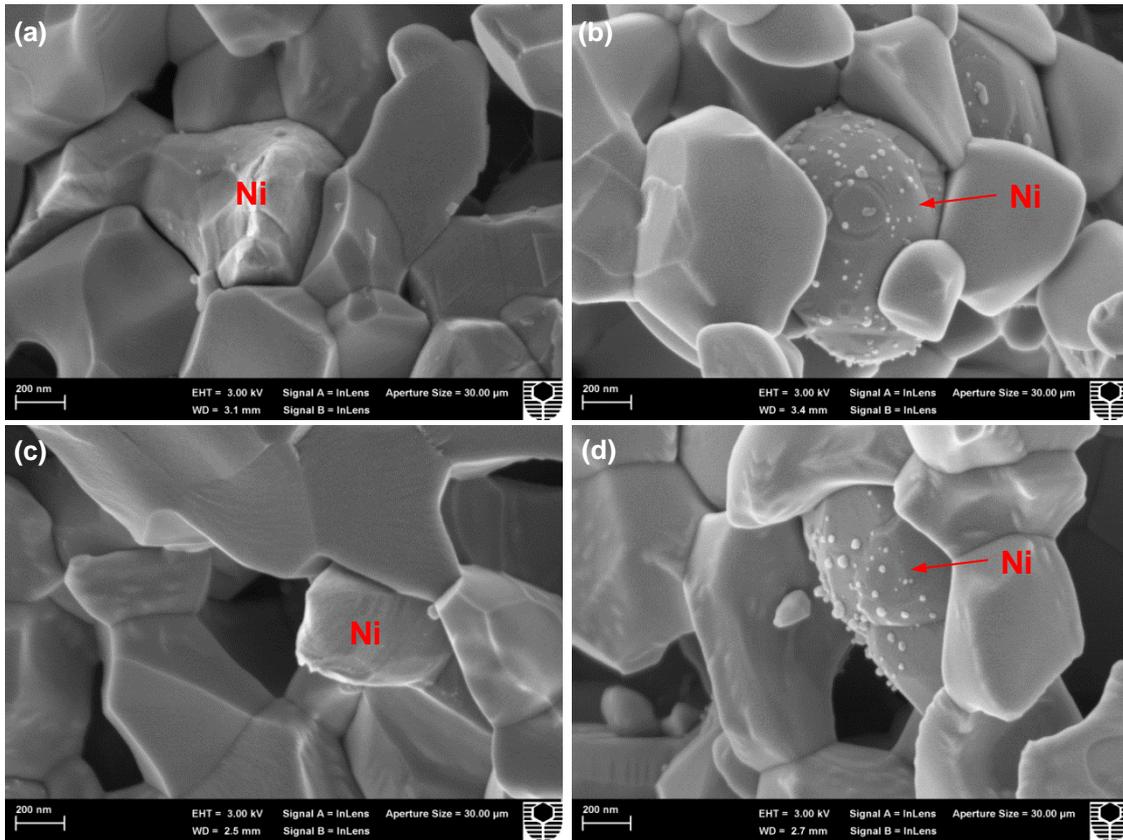
Figure 8. SEM micrographs of cross sections of Ni-YSZ anodes: (a,b) after the initial performance tests in various biogases; and (c,d) after the stability tests in B1 biogas for 3 h and B2 biogas for 3 h.

Table 1. Composition of gasification product gas (N_2 free) before, and after being reformed by the char catalyst[*].

Components	Mallee wood		Wheat straw	
	B1	A1	B2	A2
H_2	50.62	54.26	49.18	53.31
CO	17.05	18.54	16.83	17.58
CO_2	23.99	19.61	25.47	21.00
CH_4	8.34	7.59	8.52	8.12

[*]The sulphur and chlorine contents of the gasification product gases were not measured and N_2 content in the product gas was in the range of 50-64%.

Table 2. Power densities at a cell voltage of 0.7 V of the tubular cells running on different fuels at 800^oC.

Fuels / Flow rate / ml min^{-1}	Power density / mW cm^{-2}		
	25	50	100
H_2	-	523	598
CH_4	-	583	-
B1	250	363	435
B2	234	363	440
A1	288	398	436
A2	255	374	459

Table 3. Fuel efficiencies measured at cell voltage of 0.7 V of the tubular cells running on different fuels at $800^{\circ}C$.

Flow rate/ml min⁻¹ Fuels	Fuel efficiency / %						
	25		50		100		200
H_2	-		38.9		22.1		11.5
CH_4	-		10.7		-		-
B1	57.9①	80.3②	42.1①	59.2②	25.5①	35.5②	-
B2	57.7①	79.2②	44.3①	61.7②	26.8①	37.6②	-
A1	62.2①	87.1②	44.5①	59.7②	23.6①	32.3②	-
A2	58.2①	81.0②	43.0①	59.5②	26.6①	36.7②	-

① N_2 content is 50%; ② N_2 content is 64%.